The anticancer and EGFR-TK/CDK-9 dual inhibitory potentials of new synthetic pyranopyrazole and pyrazolone derivatives: X-ray crystallography, *in vitro*, and *in silico* mechanistic investigations

Arafa Musa[1*¥], Saleh K. Ihmaid[2], David L. Hughes[3], Musa A. Said[4], Hamada S. Abulkhair[5,6*], Ahmed H. El-Ghorab[7], Mohamed A. Abdelgawad[8], Khaled Shalaby[9], Mohamed E. Shaker[10], Khalid Saad Alharbi[10], Nasser Hadal Alotaibi[11], Deborah L. Kays[12], Laurence J. Taylor[12], Della Grace Thomas Parambi[8], Sami I. Alzarea[10], Ahmed A. Al-Karmalawy[13], Hany E. A. Ahmed[5¥], Ahmed M. El-Agrody[14]

[1] Department of Pharmacognosy, College of Pharmacy, Jouf University, Sakaka, Aljouf 72341, Saudi Arabia; akmusa@ju.edu.sa

[2] Pharmaceutical Chemistry Department, Faculty of Pharmacy, Jadara University, Irbid, Jordon; saleh_ihmaid@yahoo.com.au

[3] School of Chemistry, University of East Anglia, Norwich NR4 7TJ, UK; d.l.hughes@uea.ac.uk

[4] Chemistry Department, College of Sciences, Taibah University, Al-Madinah Al-Munawarah 41477, Saudi Arabia; masaid@taibahu.edu.sa

[5] Pharmaceutical Organic Chemistry Department, Faculty of Pharmacy, Al-Azhar University, Nasr City, Cairo, Egypt; hamadaorganic@azhar.edu.eg; heahmad@azhar.edu.eg

[6] Pharmaceutical Chemistry Department, Faculty of Pharmacy, Horus University-Egypt, International Coastal Road, New Damietta 34518, Egypt; habulkhair@horus.edu.eg

[7] Department of Chemistry, College of Science, Jouf university, Sakaka, Aljouf 72341, Saudi Arabia; aghorab@ju.edu.sa

[8] Department of Pharmaceutical Chemistry, College of Pharmacy, Jouf university, Sakaka, Aljouf 72341, Saudi Arabia; mhmdgwd@ju.edu.sa, dellajesto@gmail.com

[9] Department of Pharmaceutics, College of Pharmacy, Jouf University, Sakaka 72341, Saudi Arabia; khshalabi@ju.edu.sa; melsayed@ju.edu.sa

[10] Department of Pharmacology, College of Pharmacy, Jouf University, Sakaka, Aljouf 72341, Saudi Arabia; kssalharbi@ju.edu.sa, samisz@ju.edu.sa

[11] Department of Clinical Pharmacy, College of Pharmacy, Jouf University, Sakaka, Aljouf 72341, Saudi Arabia; nhalotaibi@ju.edu.sa

[12] School of Chemistry, University of Nottingham, University Park, Nottingham, NG7 2RD, UK; deborah.kays@nottingham.ac.uk; laurence.taylor@nottingham.ac.uk

[13] Pharmaceutical Chemistry Department, Faculty of Pharmacy, Ahram Canadian University, 6th of October City, Giza 12566, Egypt; akarmalawy@acu.edu.eg

[14] Chemistry Department, Faculty of Science, Al-Azhar University, Nasr City, Cairo, Egypt; elagrody_am@azhar.edu.eg

¥ These authors contributed equally to this work and share the first authorship.

Correspondence: Arafa Musa; Department of Pharmacognosy, College of Pharmacy, Jouf University, Sakaka, Aljouf 72341, Saudi Arabia.; E-mail: akmusa@ju.edu.sa

Correspondence: Hamada S. Abulkhair; Pharmaceutical Organic Chemistry Department, Faculty of Pharmacy, Al-Azhar University, Nasr City 11884, Cairo, Egypt; E-mail: hamadaorganic@azhar.edu.eg; ORCID: https://orcid.org/0000-0001-6479-4573.

Abstract:

Treatment options for the management of breast cancer are still inadequate. This inadequacy is attributed to the lack of effective targeted medications, often resulting in the recurrence of metastatic disorders. Cumulative evidence suggests that epidermal growth factor receptor (EGFR-TK) and cyclin-dependent kinases-9 (CDK-9) Overexpression is associated with a lower overall survival rate in breast cancer patients. Pyranopyrazole and pyrazolone are privileged options for the development of anticancer agents. Inspired by this proven scientific fact, we report here the synthesis of two new series of suggested anticancer molecules incorporating both heterocycles together with their characterization by IR, ^{1}H NMR, ^{13}C NMR, ^{13}C NMR-DEPT, and X-ray diffraction methods. An attempt to get the pyranopyrazole-gold complexes was conducted but unexpectedly yielded benzylidene-2,4-dihydro-3*H*-pyrazol-3-one instead. This unexpected result was confirmed by X-ray crystallographic analysis. All newly synthesized compounds were assessed for their anti-proliferative activity against two different human breast cancer cells, and the obtained results were compared with the reference drug Staurosporine. The target compounds revealed variable cytotoxicity with IC_{50} at a low micromolar range with superior selectivity indices. Target enzyme EGFR-TK and CDK-9 assays showed that compounds **22** and **23** effectively inhibited both biological targets with IC_{50} values of 0.143 and 0.121 μM, respectively. Both molecular docking experiments and molecular dynamics simulation were also conducted for further interpretations of the *in vitro* obtained results.

Keywords: Crystal structure**;** Phenylpyrazole; Pyrazolone; EGFR-TK; CDK-9; Anticancer; Molecular dynamics

1 Introduction

Breast cancer continues to terminate women's lives globally. On February 2022, The WHO reported that the incidence of breast cancer is more than two million cases, with about 685,000 deaths occurring in 2020 [1]. Over the past few years, various strategies have been provided for prevention of breast cancer development and to halt patient deterioration. The over-expression and/or mutation of epidermal growth factor receptor tyrosine kinases (EGFR-TK) subtype in breast cancers have a great effect in cancer development and growth, these effects are metastasis, cell proliferation, angiogenesis and anti-apoptosis [2–5]. EGFR-TK thus has been proved to be a sticking target for the development of breast cancer chemotherapeutics [4,5]. Accordingly, a number of chemotherapeutic drugs like imatinib (**1**; **Figure S1; see supplementary file**), afatinib (**2**), erlotinib (**3**), and gefitinib (**4**) have been introduced globally to treat this malignant disease [4,6]. The primary goal of these medications' action targets is to affect the EGFR-TK signal transduction pathway [7,8]. On the other hand, cyclin-dependent kinases (CDKs) also play a pivotal role in the regulation of the cell cycle. They are overexpressed in various malignant tumors including breast cancer in particular [9]. One of the crucial CDKs that is included in cellular transcription elongation and gene transcription is the CDK-9. Accordingly, CDK-9 has long been considered one of the main targets for cancer management [10]. The inhibition of CDK-9 with atuveciclib (**5**) has been proved as an effective strategy to reduce cell proliferation and survival of breast cancer cells [11]. To date, three CDK inhibitors have been previously authorized by the FDA for the management of different malignancies. These include palbociclib (**6**), ribociclib (**7**), and abemaciclib (**8**) [12]. CDK-9 inhibitors downregulate the anti-apoptotic family of myeloid cell leukemia-1 (MCL-1) and hence could alleviate breast cancer cells [13,14].

Arylpyrazoles are active motifs that possess various biological activities including anti-inflammatory [15], anticonvulsant [16,17], anticancer [18–20], antiviral [21], and neuroprotective activity [22]. In the present year, a series of *N*-arylpyrazoles has been

synthesized and estimated as potential anticancer candidates for breast (MCF-7 & MDA MB-231), lung (A549), prostrate (DU-145) cancers. Among the synthesized arylpyrazoles, compounds **9** and **10** (**Figure 1**) demonstrated more potent activity than etoposide. In particular, compound **10** showed the best efficiency compared to all other derivatives [IC_{50} = 0.31 μM (MCF-7), 0.37 μM (MDA MB-231), 0.47 μM (A549), and 0.19 μM (DU-145)] [19]. As well, many *N*-arylpyrazole derivatives have been synthesized through one-pot two-steps consecutive methodology. The produced *N*-arylpyrazoles were evaluated *in vitro* for their potential anticancer activity against a panel of eight human cancer cells including breast cancers (MCF-7). The *N*-phenylpyrazoles **11** and **12** exhibited good growth inhibitory activity against breast cancer cells with GI_{50} values of 72.44 μM and 74.15 μM, respectively, with acceptable selectivity indices. They also showed good potential to interact with the crucial amino acid residues of the CDK target in the performed docking experiments [19]. On the other hand, numerous *N*-arylpyrazoles have been recently developed and presented good inhibitory activity against certain subtypes of CDKs [23,24]. Among these, **13** and **14** displayed better cytotoxicity than imatinib on MCF-7 breast cancer cell line with IC_{50} values of 3.0 μM and 4.0 μM, respectively. The former one demonstrated outstanding inhibitory activity against CDK-2 with IC_{50} value of 0.24 μM (62.5% inhibition in relative to imatinib) [25].

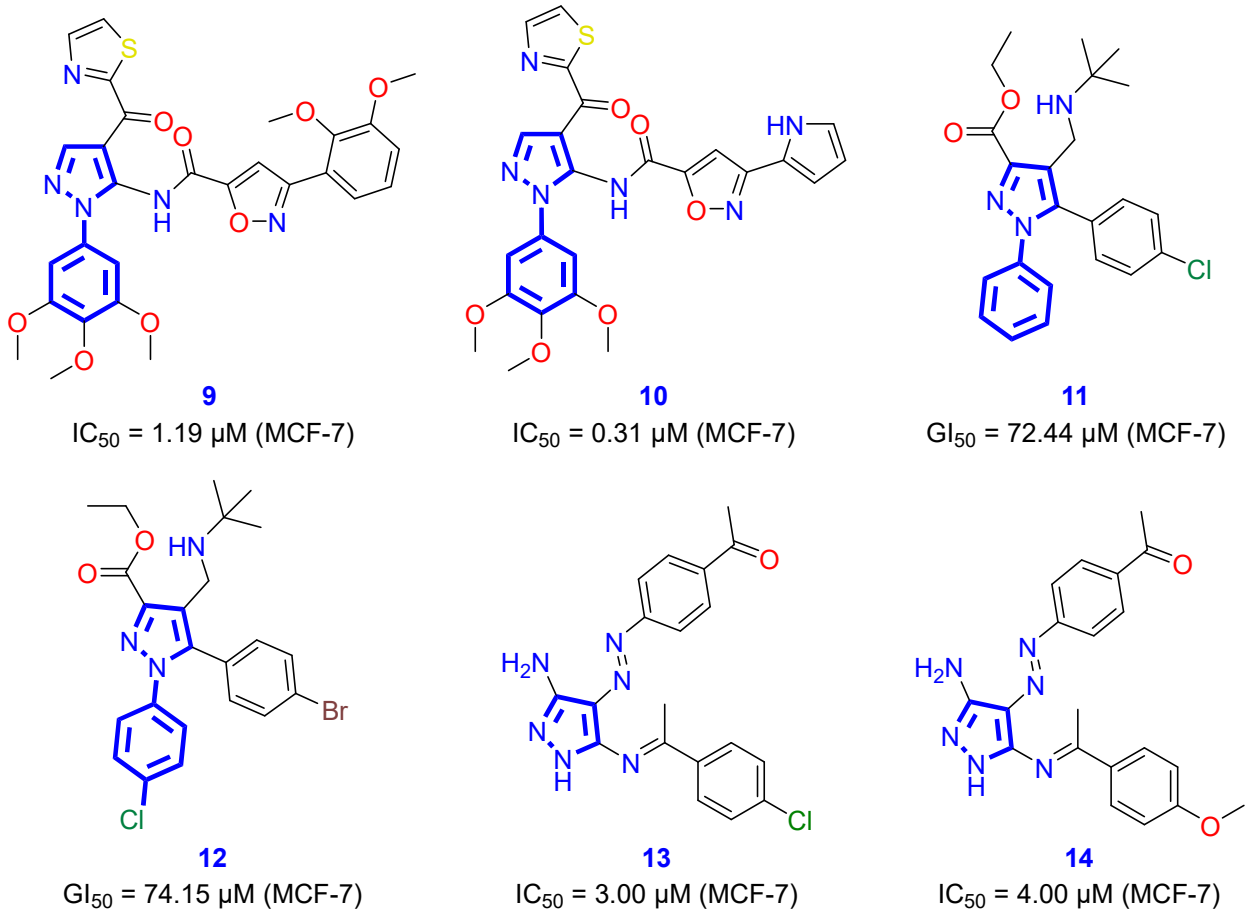

Figure 1: Arylpyrazoles as effective anticancer candidates targetting EGFR-TK and CDK

1.1 Rational design and aim of the work

Our recent studies have led to the identification of benzopyran and pyranopyrazole scaffolds as a promising fused ring system with good anticancer activity [26–29]. They were designed with terminal aromatic lipophilic moiety and prepared through a one-pot three-component reaction. In the present work, inspired by the above proven scientific findings and in continuation of our recent records in the synthesis of bioactive heterocycles , we prepared a new set of suggested anticancer pyranopyrazoles with prominent activity against breast cancer cells. Driven by the tremendous advances in the development of anticancer gold-containing complexes [30,31], we tried to get a set of pyranopyrazole-gold coordinates by reacting this set with gold(III) chloride hydrate. Unexpectedly, an alternative set of benzylidene-2,4-dihydro-3*H*-pyrazol-3-ones has been

obtained instead. Consequently, we presented a proposed mechanism for the formation of the unexpected products. The single-crystal structure of one product was also confirmed through X-ray crystallography and different spectroscopic techniques. The newly synthesized molecules were evaluated for their antiproliferative effect on various invasive and non-invasive breast cancers (MCF-7andMDA-MB-231). For assessing the selectivity indices of target pyranopyrazoles and the obtained benzylidene-2,4-dihydro-3*H*-pyrazol-3-one toward cancer cells, their cytotoxicity on normal cell lines, namely, Michigan Cancer Foundation-10A (MCF-10A) were also investigated. Then, the proposed mechanistic effect of these new compounds was also evaluated *in vitro* against two chemotherapeutic targets. Lastly, docking experiments and molecular dynamics simulations (MD) of the new compounds on EGFR-TK/CDK-9 were also conducted to further rationalize the obtained results of *in vitro* bioactivity.

2 Results and discussion

2.1 Chemistry

The target compounds (**18-20**) were synthesized as represented in **Scheme 1**. pyrano[2,3-*c*]pyrazole derivatives (**18-20**) were easily attained in a satisfactory yield by a one-pot, three-component reaction of precursor phenylpyrazole **(15)**, malononitrile **(16)** with three aromatic aldehydes (**17**) in an ethanolic solution containing a catalytic amount of piperidine. Alternatively, the target compounds (**18-20**) were also obtained by condensation of precursor phenylpyrazolone (**15**) with the same set of aldehydes (**17**) to afford the benzylidene-pyrazolone (**21-23**). These latter were lastly allowed to react with malononitrile (**16**) to give our target pyranopyrazoles (**18-20**).

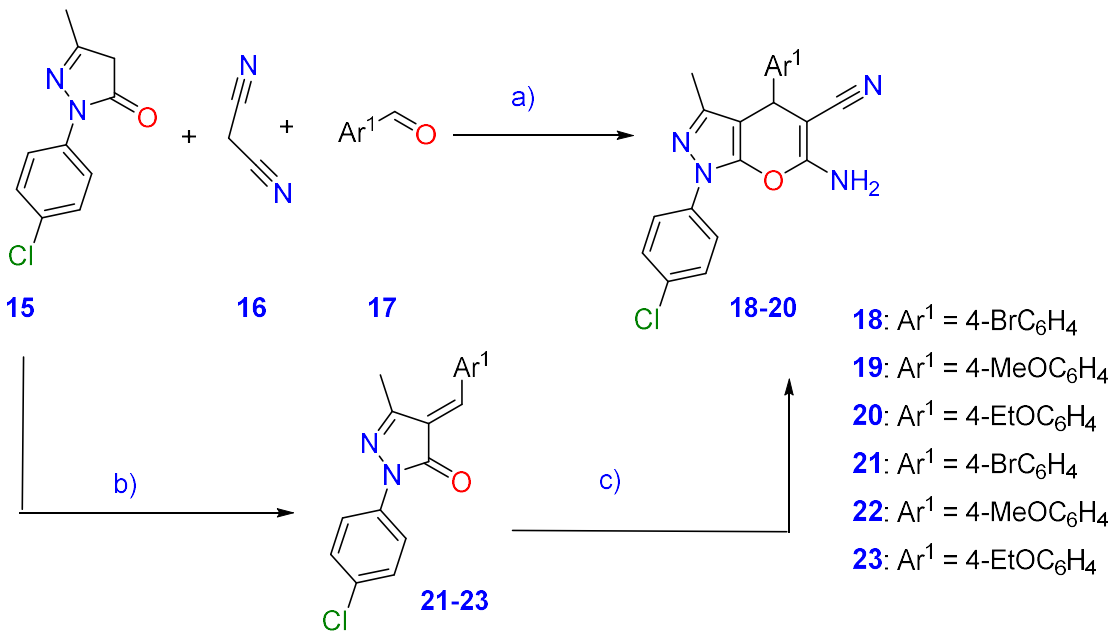

Reagents and conditions

a) C_2H_5OH, piperazine, 100°C, 1 hr

b) ArCHO, C_2H_5OH, 100°C, 1 hr

c) $CH_2(CN)_2$, C_2H_5OH, piperazine, 100°C, 1 hr

Scheme 1: Synthesis of target pyranopyrazoles and pyrazolone derivatives (**18-23**)

The history of gold complexes as homogeneous catalysts indicates a very successful and attractive area of chemistry [32–34]. In a preliminary plan, our group tested the action of gold (III) chloride hydrate reagent on aryl pyrano[2,3-*c*]pyrazole-5-carbo-nitrile **(18)**, in ethanol containing few drops of triethylamine; the product was 4-bromobenzylidene-pyrazol-5(4*H*)-one **(21)** in low yield as red crystals, rather than the gold complex **(24), Scheme 2**.

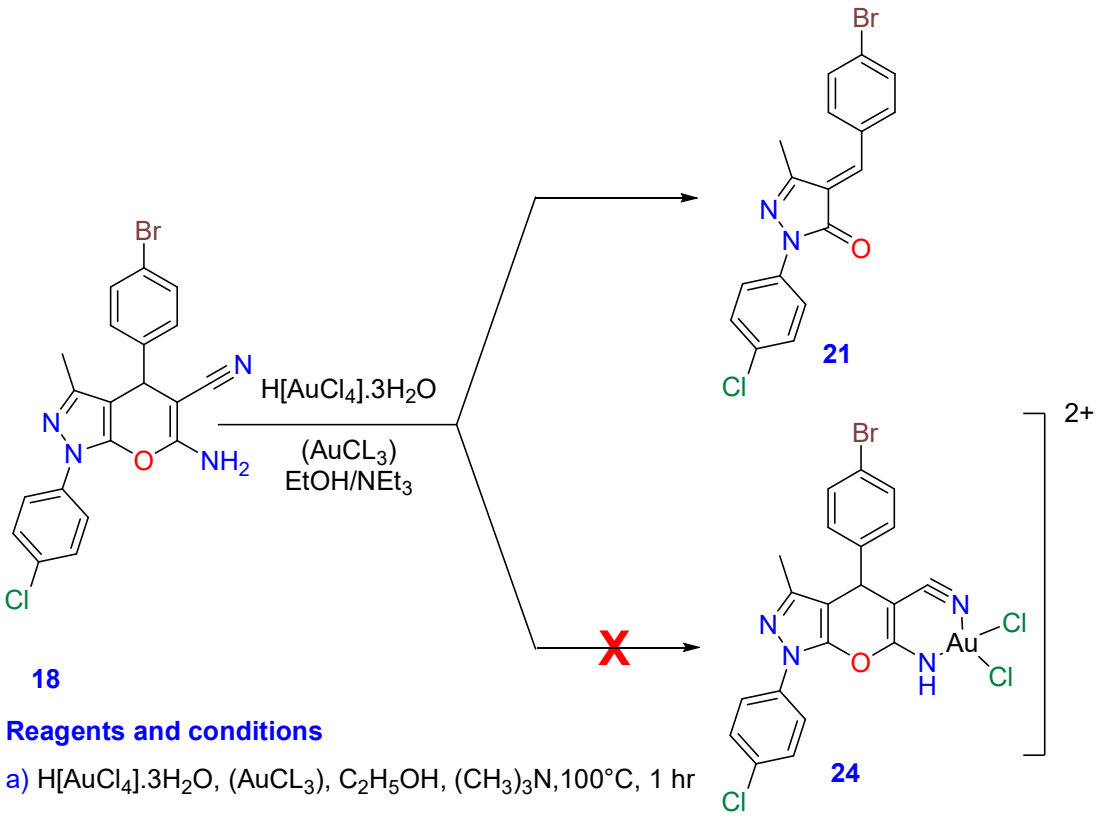

Scheme 2: Synthesis of target compound **21**

A mechanism for the formation of product (**21**) under the catalytic effect of gold (III) chloride hydrate is depicted in **Scheme 3**. The catalytic effect of $HAuCl_4$ hydrates is due to the dissociation equation as follow:

$$H[AuCl_4].3H_2O \rightleftharpoons HCl + AuCl_3 + 3H_2O$$

It is, therefore, not surprising that for certain reactions, $AuCl_3$ is a better catalyst than a $HAuCl_4$ hydrate [35]. The formation of compound **21** is supposed to proceed *via* the nucleophilic opening of the pyran ring [36], followed by transformation into the pyrazolone intermediate (**25**), which then undergoes retro-decomposition [37,38] to form Benzylidenepyrazol-5(4*H*)-one **(21)** and malononitrile **(16), Scheme 3.**

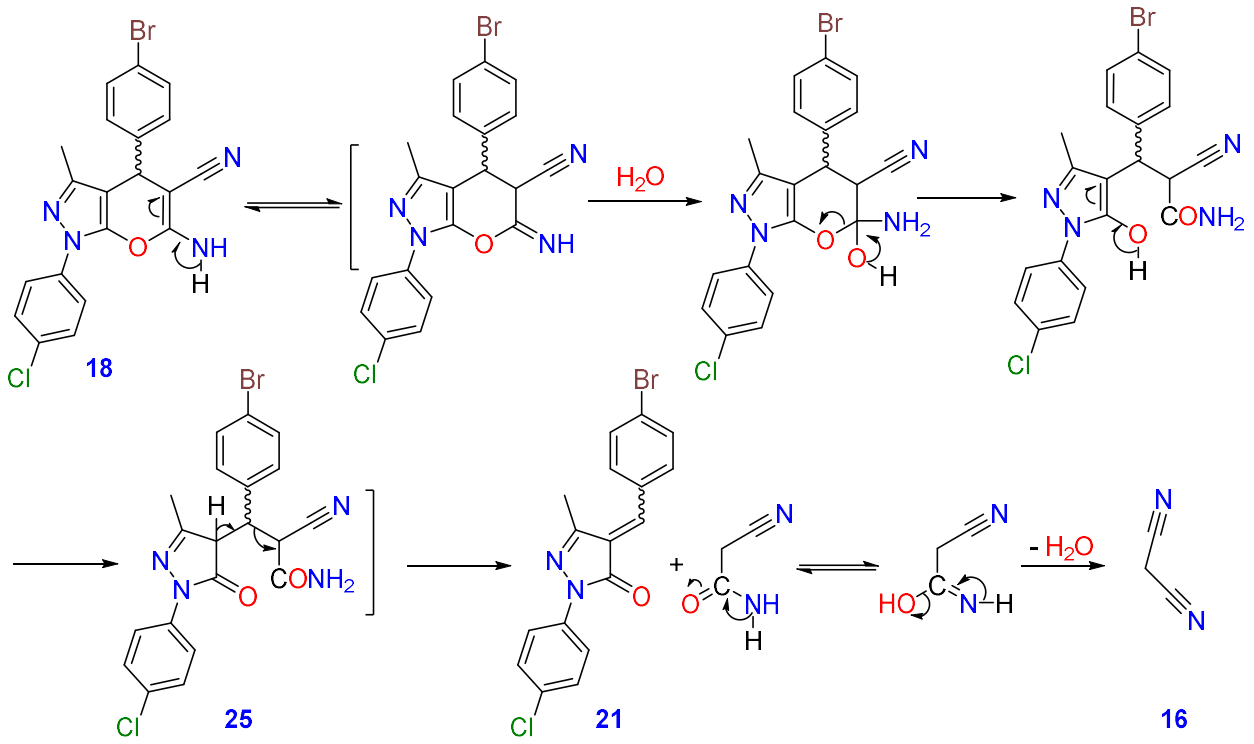

Scheme 3: Suggested chemical analysis synthesis of final product **21**

2.2 *Optical activities*

Compounds **18-20** are chiral. So, their specific rotation was measured using a Carl Zeiss polarimeter to adjust the 4-position stereochemistry of the pyrano[2,3-*c*]pyrazole moiety. The results indicated that these derivatives are optically inactive with zero rotation present in a racemate (±) mixture [26,39,40].

2.3 *Spectroscopic data*

The structures of compounds **18-20** and **21-23** were in great consistence with obtained spectroscopic data and the elemental analyses . The IR spectra disclosed absorption bands around υ 3492-3428, 3385-3361, 3232-3230 cm^{-1} for NH_2 in addition to cyano groups absorption bands in the region υ 2189-2182 cm^{-1} for compounds **18-20** and the absorption maxima of carbonyl groups lies in the region of υ 1705-1701 cm^{-1} for compounds **21-23.** Also, the ^1H NMR spectra of **compounds 18-20** resulted in diverse signals of the function groups; methine, amino, and methyl protons in the range of δ 7.31-7.20, 4.62-4.71, 1.79-

1.78 ppm, respectively and the ^{13}C NMR spectra exhibited the methine carbons signals in the range δ 58.05-55.48 ppm for compounds **18-20** and the carbons of carbonyl and olefinic groups at δ 164.25, 163.17 and 146.91, 148.69 ppm for compounds **22,** respectively. Moreover, the ^{13}C NMR-DEPT spectrum at 135°, HPLC-Mass Spectrometry for compounds **18-20, 21-23,** and single-crystal X-ray analysis of compound **21** strongly confirmed the structure and the absolute configuration of target compounds (see experimental section and supplementary file).

2.4 The X-ray characterization of compound 21.

Single-crystal X-ray diffraction was done and characterized unexpected product **21** . The crystal structure shows disorder with the major component (66.2%) overlaying the minor component (33.8%). Each component in the structure is essentially planar; in the major component, each of the three-ring groups forms a good plane with a twist of 7.55(12)° between the normals to the C(51-56) phenyl ring and the central pyrazolone ring; the angle between the normals to the second phenyl ring C(21-26) and the central pyrazolone ring is 9.5(2)°, (**Figure 2)**.

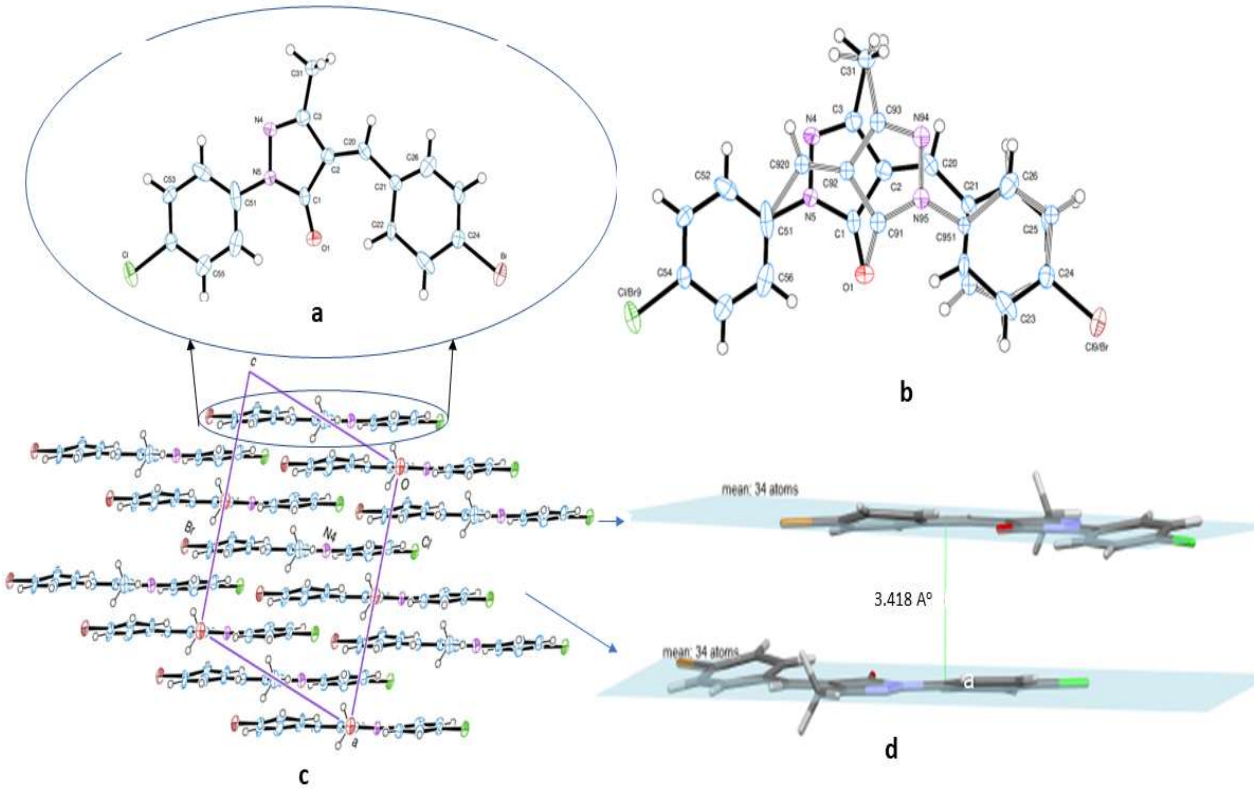

Figure 2: (a) View of the major component of **21**, showing the atom numbering scheme. Thermal ellipsoids (n 50% probability level); (b) Components of the disordered molecule **21**; (c) The packing of molecules viewed along the b axis; (d) shows the distance between two planes

The minor component is related to the major by a pseudo-twofold symmetry axis that passes through O(1) and C(31), sites common to both components. Other atoms in the two components that are coincident are C(24) and C(954), C(26) and C(954), Br and Cl(9), and Cl and Br(9); the two overlapping rings of C(21-26) and C(951-956) are quite distinct and resolved, but the corresponding pair of C(51-56) and the minor phenyl group on C(920) have not been resolved but were refined as a single, fully occupied six-membered ring. In the pyrazolone ring of the major component, there are, in addition to the carbonyl group, C(1)–O(1) 1.257(7) Å, short, double-bond contacts between C(3)–N(4), 1.271(12) Å and C(2)–C(20) 1.365(11) Å. Molecules (involving both components) are stacked by $\pi\ldots\pi$ interactions parallel to the *a* axis; adjacent molecules are related by the glide-plane symmetry of the structure. The experimental details for the measurement of diffraction

data, processing of the data, structure solution (by intrinsic phasing methods), and refinement of **21** are recorded in **Table 1**. Selected angles and bond lengths are listed in **Table S1 in the supplementary file**.

Table 1: Crystallographic data and structure refinement for the pyrazolone derivative, **21**

Elemental formula	$C_{17}H_{12}BrClN_2O$
Formula weight	375.65
Crystal system, space group	Monoclinic, C c (no. 9)
Unit cell dimensions	a = 10.5759(5) Å α = 90°
	b = 14.0729(5) Å β = 105.502(4)°
	c = 10.3189(4) Å γ = 90°
Volume	1479.93(11) Å3
Z, Calculated density	4,1.686 Mg/m3
F(000)	752
Absorption coefficient	5.467 mm-1
Temperature	120(2) K
Wavelength	1.54184 Å
Crystal colour and shape	red blocks
Crystal size	0.148 x 0.110 x 0.092 mm
Crystal mounting:	on a glass fibre, in oil, fixed in cold N2 stream
On the diffractometer:	
Theta range for data collection	5.359 to 67.452 °
Limiting indices	-12<=h<=12, -16<=k<=14, -12<=l<=11
Completeness to theta = 67.452	99.9%
Absorption correction	Gaussian
Max. and min. transmission	1.000 and 0.835
Reflections collected (not including absences)	2634
No. of unique reflections	1690[R(int)for equivalents = 0.012]
No. of 'observed' reflections (I > 2σI)	1668
Structure determined by:	dual methods, in SHELXT
Refinement:	Full-matrix least-squares on F2, in SHELXL
Data/restraints/parameters	1690 / 2 / 242
Goodness-of-fit on F2	1.054
Final R indices ('observed' data)	R1 = 0.022, wR2 = 0.057
Final R indices (all data)	R1 = 0.023, wR2 = 0.058
Reflections weighted:	
w = [σ2(Fo2) + (0.0293P)2 +1.1085P]-1 where P = (Fo2 + 2Fc2)/3	

Absolute structure parameter	0.20(3)
Extinction coefficient	n/a
Largest diff. peak and hole	0.22 and -0.30 e.Å-3
Location of largest difference peak	near Br

2.5 Biological evaluation.

2.5.1 Assay of Cell proliferation and SAR analysis

The interesting compounds were assessed by using an *in vitro* anti-cancer activities against three different breast cancer cell lines: MCF-7 (Michigan Cancer Foundation-7, Invasive ductal carcinoma), MDA-MB-231 (Breast Adenocarcinoma) and MCF-10A (a human normal breast cell), following the MTT assay technique [41–43]. Staurosporine was applied as the standardized positive effective therapy in breast cancer [44,45] to compare its cytotoxic effect with those obtained by our targeted compounds. IC_{50} of both target compounds and positive control are presented in **Table 2**. The IC_{50} results revealed variable responses to various cell lines. The growth inhibitory responses of compounds **18-20** and **21-23** on the tested cell lines are also discussed.

In general, the benzylidene derivatives **21-23** are more potent as cell cytotoxic compared to pyranopyrazole derivatives **18-20**. Compound **18** has only 27% cytotoxic activity compared to the control in MCF-7 and ~25% in the MD-MB-231 breast cancer cell line, while compound **19** has ~ 42% cytotoxicity in both MCF-7 and MDA-MB-231 cell lines in comparison with the positive control. However, compound **20** shows ~93% growth inhibitory activity in MCF-7 and ~65% in MDA-MB-231 relative to the positive control, thus highlighting the selectivity of this compound for MCF-7 cell lines. Regarding the benzylidene derivatives, compound **21** showed a relatively weak cytotoxic activity in reference to the positive control against MCF-7 and MDA-MB-231 cell lines based on their IC_{50} values. The methoxy derivative **22** shows ~65% and 45% growth inhibition for MCF-7 and MDA-MB-231 respectively, which indicates that **22** is more

selective for MCF-7 than MDA-MB-231. For the ethoxy benzylidene derivative **23,** the growth inhibitory activity in MCF-7 is more than twice as potent than the +ve control and nearly twice as potent in the MDA-MB-231 cell lines; this all reflects the high potency of this benzylidene derivative.

Table 2: *In vitro cellular* antiproliferation effects of the target compounds, and Staurosporine on different breast cancer cell lines.

Cpd. ID	MTT assay IC_{50} ($\mu g/mL$) [1]			Selectivity pattern
	MCF-7	MDA-MB-231	MCF-10A	
18	21.55 ± 1.28	35.14 ± 1.85	ND[2]	Active
19	13.85 ± 0.82	21.87 ± 1.15	ND	Active
20	6.32 ± 0.37	13.88 ± 0.73	102.00 ± 1.41	MCF-7 selective
21	29.44 ± 1.74	57.25 ± 3.02	ND	Less active
22	9.04 ± 0.54	20.29 ± 1.07	ND	MCF-7 selective
23	2.60 ± 0.15	5.14 ± 0.27	85.00 ± 2.15	Potent active
Staurosporine	5.86 ± 0.35	9.02 ± 0.47	ND	

[1] IC_{50} values are expressed mean ± standard error values of triplicates. P-value is < 0.05.

[2] ND = Not Determined

2.5.2 Enzyme assay

The inhibition of EGFR-TK (epidermal growth factor receptor) and Cyclin-dependent kinase 9 (CDK-9) plays a crucial role in tumor suppression in breast cancer [2–5] [9]. All synthesized compounds were estimated for their *in vitro* EGFR-TK and CDK-9 inhibitory activities, and the IC_{50} values were calculated and compared to the reference drugs Lapatinib and Dinaciclib, respectively, **Table 3**. As seen, the benzylidene derivatives **22** and **23** are stronger inhibitors for both EGFR-TK and CDK-9 compared to the dihydropyrano derivatives **18-20**. Also, the alkyloxy derivatives **19** and **20** in both groups are more effective inhibitors than the bromo derivatives; this emphasizes the importance of the bromo substituent type on the activity. Compound **22** shows a promising inhibitory

effect against EGFR-TK with compound **23** showing the highest inhibition against EGFR-TK compared to the reference drug Lapatinib. With respect to the inhibitory activity against CDK-9 also **22** and **c** show the highest inhibition activity close to the drug Dinaciclib.

Lipophilic characters of a compound are a good indicator of its potency. However, a balance between lipophilic and hydrophilic character is important for drugs to be orally active. Compounds with 2-3.5 lipophilic value range are optimal as oral drugs with prominent good bioavailability.. Leeson *et al*., has introduced the lipophilic efficiency concept(LPE), which measures how well a ligand uses the lipophilic property to attach to a specific target, and which brings together both potency and lipophilic properties as a criterion of drug-likeness. It could be used to increase drug potency without increasing Log P [46]. For further exploration of that concept for both EGFR-TK and CDK-9 inhibitors, LPE values for the various derivatives and a reference drug have been calculateds, **Table 3**. The Log *P* values vary from 1.40 to 5.39, leading to a lipophilic efficiency range between 1.30 and 4.00 for EGFR-TK and 0.20 to 5.70 for CDK-9. Moreover, the improved solubility factors appeared in results of compounds and reference drugs increased the potential to be proper pharmacokinetic profile for these derivatives. This particular characteristic controlled the possibility of penetration and the relative excellent oral absorption. Table 3 illustrated that the target compounds 22 and 23 have acceptable LPE 2.70 and 3.6, respectively compared with the selected reference drugs.

2.6 EGFR-TK target docking simulations

Docking studies are now a very important part of the process for the design and optimization of drug. [47–51].firstly, the **21**, **22**, and **23** compounds were docked into the crystal structure compared to bound ligand and exhibited binding energy range; -6.75, -7.01, -7.41, and -8.50 respectively. Focusing on the compound **23** which showed excellent

EGFR-TK inhibition to further justify the observed inhibitory activity. Previous studies [52–55] have indicated that 4-anilinoquinazoline-based drugs as Erlotinib affect their inhibitory mechanism through block of ATP-binding site. Erlotinib was found to locate well in the ATP pocket and is linked to Met769 by a hydrogen bond, at 3.09Å to nitrogen atom of the quinazoline ring at position 1, and hydrophobic interactions with Leu694 with an aromatic ring at contact distance of 4.11Å with C-C stabilization through Gln767 residue (**Figure 3**). Compound **23** interacts within the active sitethrough the pyrazolone group by a hydrogen bond with crucial amino acid Met769 through its carbonyl group within a distance of 3.25Å. There are two additional hydrophobic interactions with amino acids Leu694, and Gly772 (at distances of 4.22 and 4.77Å, respectively). This interaction pattern confirms that the pyrazolone fragment is an isostere of the quinazoline ring. The 3D overlapping of compound **23** and the reference drug Erlotinib shows the alignment of both compounds within the ATP binding region of the EGFR-TK. These findings might indicate the potential of compound **23** as a new lead that merits further structural optimization in designing new anticancer agents.

Table 3: *In vitro* dual inhibitory effect on EGFR-TK wild type and CDK-9 (IC_{50}, μM) of new candidates

Cpd. ID	Target enzyme assay*		Log P	Log S	LPE	
	EGFR-TK wild type	CDK-9			EGFR-TK	(CDK-9)
18	0.433 ± 0.026	5.706 ± 0.289	4.48	-6.05	1.9	0.7
19	0.265 ± 0.016	0.945 ± 0.048	3.52	-5.56	3.1	2.5
20	0.211 ± 0.013	1.260 ± 0.064	3.86	-5.23	2.8	2.0
21	0.200 ± 0.012	2.587 ± 0.131	5.39	-6.65	1.3	0.2
22	**0.143 ± 0.009**	**0.402 ± 0.02**	**4.15**	**-5.36**	2.7	2.0
23	**0.121 ± 0.007**	**0.077 ± 0.004**	**4.54**	**-5.72**	2.1	3.6
Lapatinib	0.040 ± 0.002	-	4.42	-1.25	4.0	-
Dinaciclib	**-**	0.081 ± 1.23	1.40	-0.575	-	5.7

* Results are expressed as IC_{50} ± SD (μM) values in triplicates. *P*-value is < 0.05 (Log *p* of reference drugs obtained from ChemAxon).

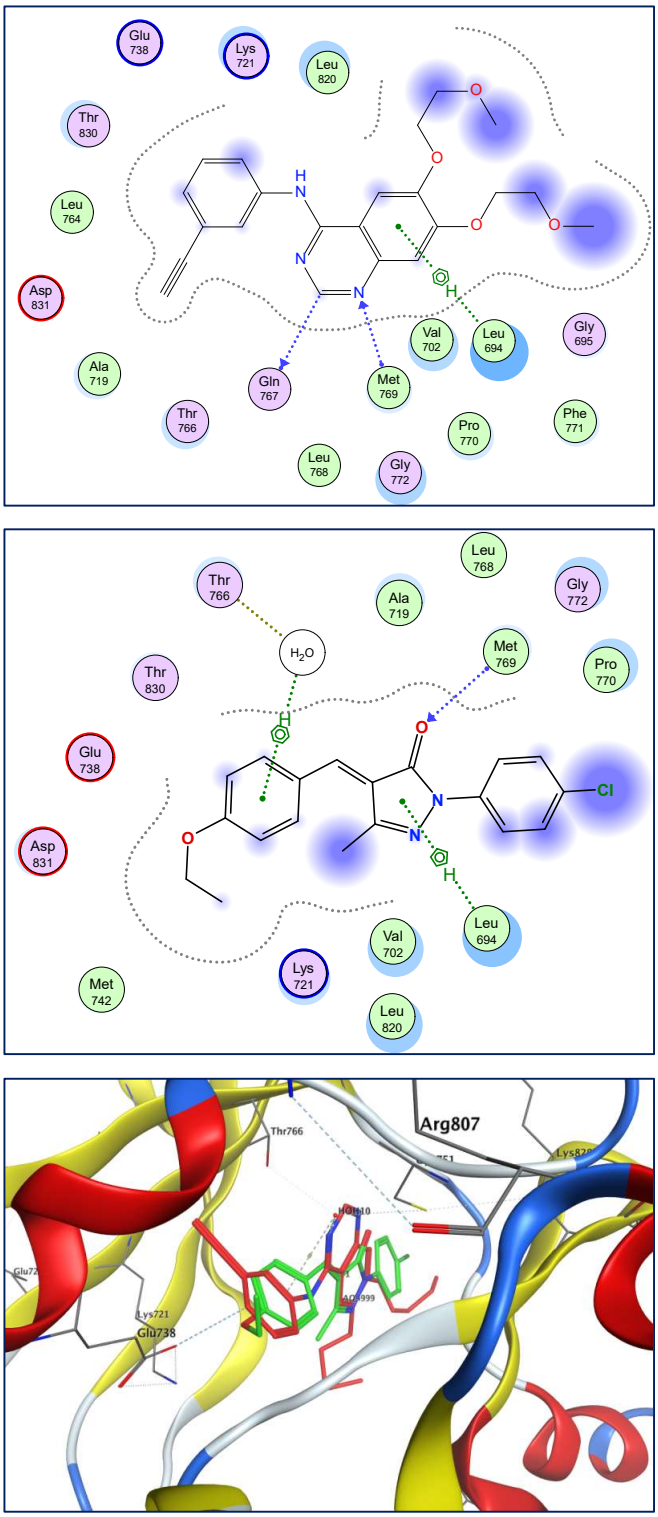

Figure 3: Docking modes of the active compound **23**. The figure shown is predicted products of Erlotinib drug with the EGFR-TK binding site (upper raw); analog **23** with the EGFR-TK ATP pocket (middle raw); 3D aligned **23**

superimposed with Erlotinib within the EGFR-TK ATP pocket (lower raw). Dashed lines are used for definition of possible hydrogen bonds between compound fragments and residues in pocket.

2.7 Molecular dynamics simulation

Both conformational changes and their stability were clearly explained through examination of protein's secondary structure of EGFR-TK coupled to the novel active analog 23 both prior to and after docking.., RMSD and RMSF data were predicted for the complex to reference EGFR-TK inhibitor and compound **23** by MD run of 100 ns [56]. Therefore, the protein's secondary structures were analyzed prior and post docking to get in depth the conformational changes resulted from ligand interaction. **Figure 4** displays the findings from the RMSD record of the EGFR-TK behavior prior to and during docking of pyranopyrazole derivative 23 and reached equilibrium after 100 ns. The acquired stable conformation of the target enzyme in the MD runs at RMSD 2Å, which is a reasonable result for a protein target enzyme and revealed the stability of the complex.

The most effective molecule 23, in association with the EGFR-TK domain, was run to evaluate the stability and dynamic behavior along the simulation durations utilizing root-mean-square deviation (RMSD). Calculations of the radius of gyration (Rg) and the number of atomic interactions (#contacts) reflected the RMSD.. From the data,

During the first 40 ns, RMSD values of the EGFR-TK/23 complex were slightly varied, these findings was strongly supported by the adaptation of atomic contacts within compound 23's five 5 spheres during this period (first 40 ns), the equilibrium of an average value of 3 RMSD was then reached after 60 ns. Moreover, in the case of co-crystallized ligand, in the first 10 ns, RMSD values was increased, followed by constant value with an average value of 1.5 RMSD until the final stage of MD simulation. During the whole simulation run and according to the Rg calculation, the compactness of the EGFR-TK domain remained constant at 20-21, which reflects the stable closed conformation of the EGFR-TK/**23** complex (**Figure 5**).

Overall, the obtained results confirmed the high stability of the produced complex of compound 23 and EGFR-TK in an aqueous environment.

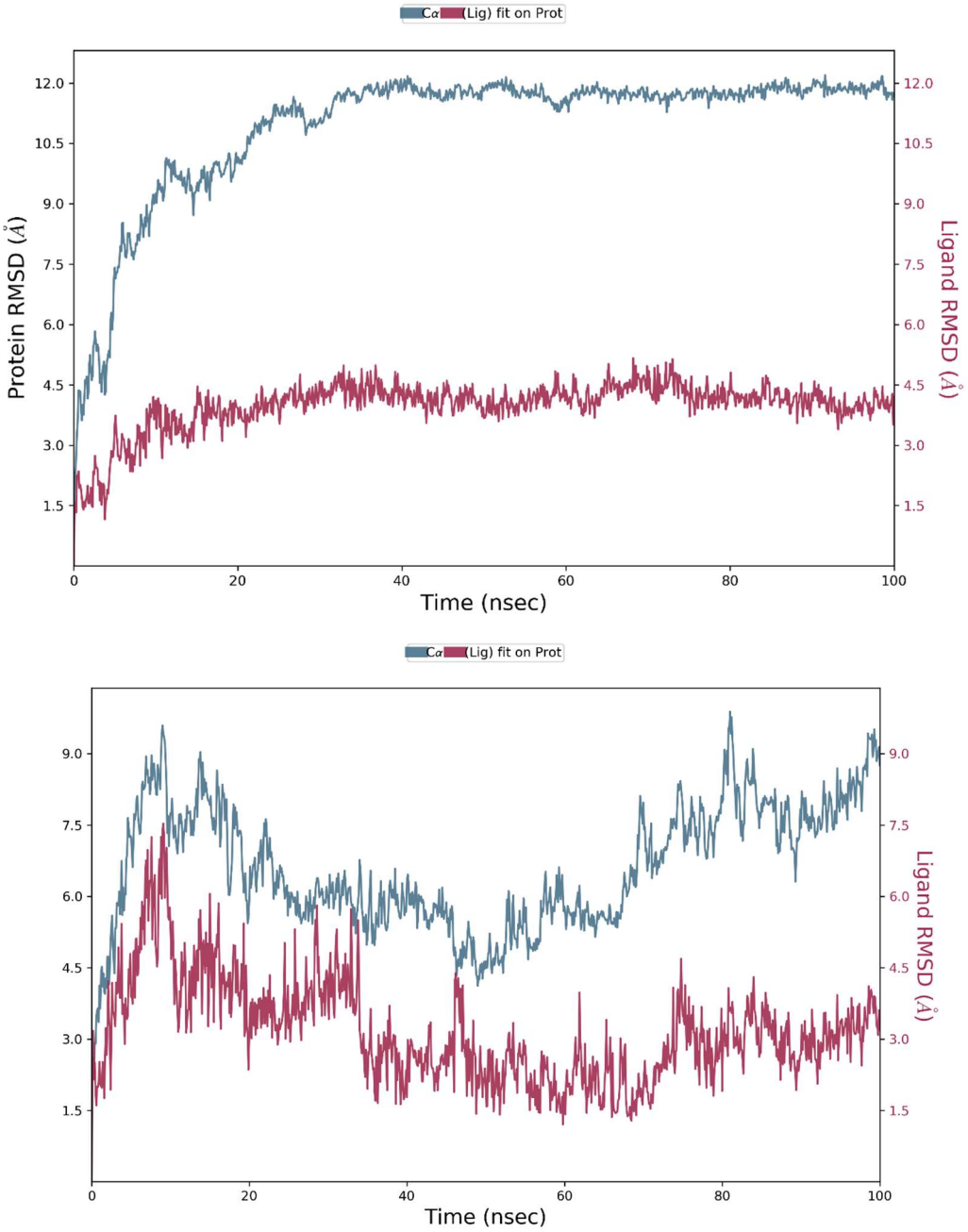

Figure 4: Results of MD of EGFR-TK (PDB ID: 1M17) complex. RMSD of complex with reference compound (upper panel) and **23** (lower panel). The stability of RMSDs was reached after 100 ns.

Both residues of N- and C-terminals were oscillated below 4.0 for compound 23 and above 3.0 for the ligand, according to the RMSF plot for EGFR with the reference ligand and compound 23. The remaining secondary structures were kept stable during the trajectory, and the protein-ligand complex's projected RMSF (Figure 5A) was less than 2.0, demonstrating conformational stability. The EGFR-TK complex with reference (Figures 5B) had a secondary structure with 26% α-helices and 15% of β-strands, whereas the complex with 23 had a secondary structure with 25.04% α-helices and 15% of β-strands. The assessment of the EGFR-TK complexes' intermolecular interactions during the MD simulation, as shown in Figures 6 A–B, showed that the studied trajectories had a range of interesting contacts of polar and non-polar interactions, supporting the findings of the docking studies. Furthermore, it was demonstrated by the plot of interaction fraction vs residues of binding sites that Met769 was the conserved residue of the given multiple interactions (interaction fraction greater than 0.3). Both molecular docking and the MD results were in great consistence, as extrapolated results revealed the involvement of the EGFR-TK complex binding site residues Met769, Cys773, Leu694, and Thr830 in hydrogen bonding for various simulation times, Figure 6B. Furthermore, it was found that the hydrophobic interactions of compound 23 with EGFR-TK complex residues (Thr766 and Leu694) were prominent through the pyrazole and terminal aromatic fragments. These interactions are consistent with the results of docking experiments and contributed to the stability of the complex for 50% of the simulation time.

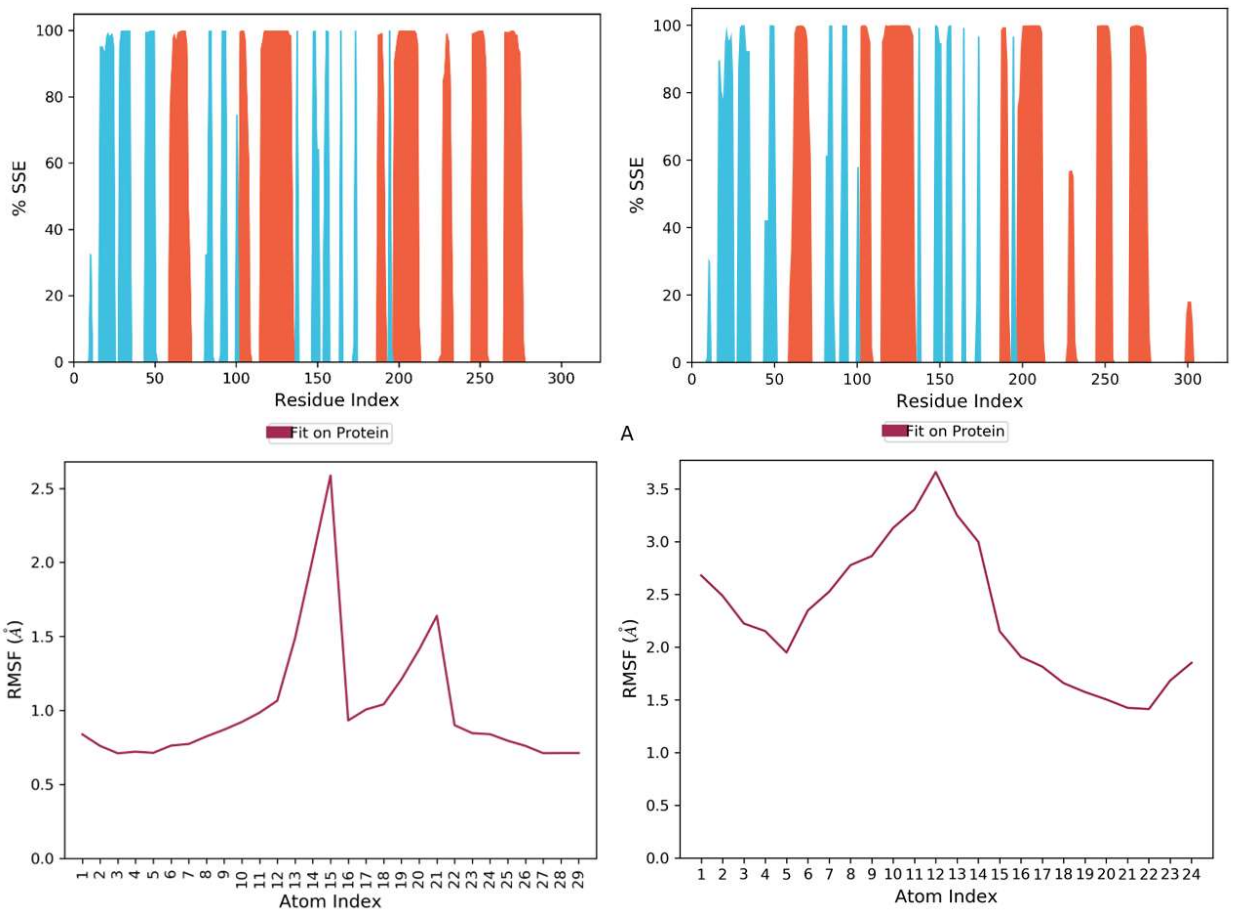

Drug	%Helix	%Strand	%Total SSE
Ref	26.91	15.59	42.50
23	25.73	15.44	41.17

Figure 5: MD data of EGFR-TK with PDB ID: 1M17) complexes. (A) Results of Ligand Root Mean Square Fluctuation (L-RMSF) for both reference (left) and **23** (right) complexed with EGFR. (B) Data of Secondary structure elements (SSE) of both reference (left) and 23 (right) complexed with EGFR. (C) Data of % SSE of the two reference and 23 compounds with EGFR-TK. It is clear shown that no changes in the percentage of SSE appears significantly between both the apo and bound proteins structures indicating their conformational stability.

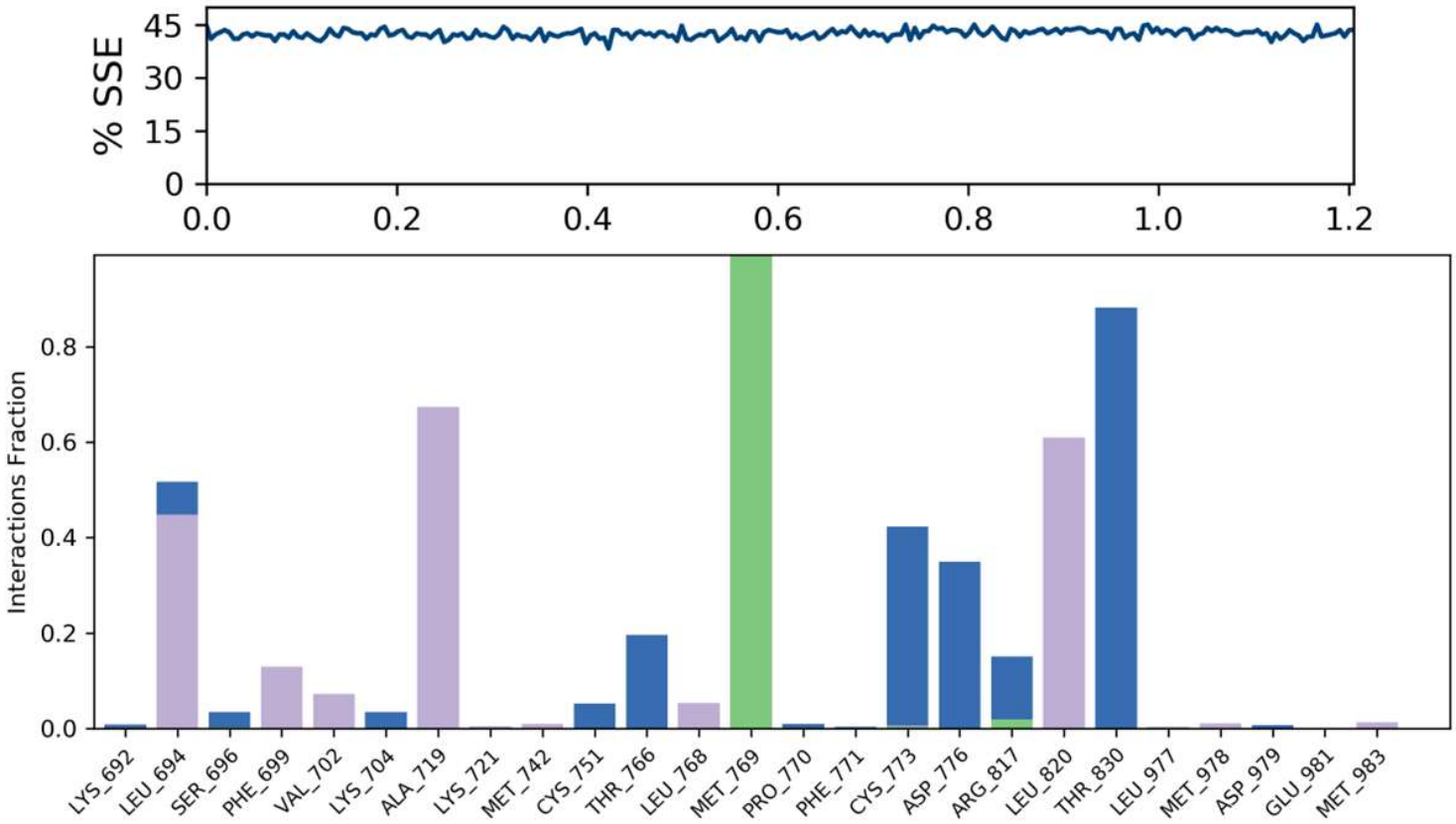
% SSE
45
30
15
0
0.0
0.2
0.4
0.6
0.8
1.0
1.2
Interactions Fraction
0.0
0.2
0.4
0.6
0.8
LYS_692
LEU_694
SER_696
PHE_699
VAL_702
LYS_704
ALA_719
LYS_721
MET_742
CYS_751
THR_766
LEU_768
MET_769
PRO_770
PHE_771
CYS_773
ASP_776
ARG_817
LEU_820
THR_830
LEU_977
MET_978
ASP_979
GLU_981
MET_983

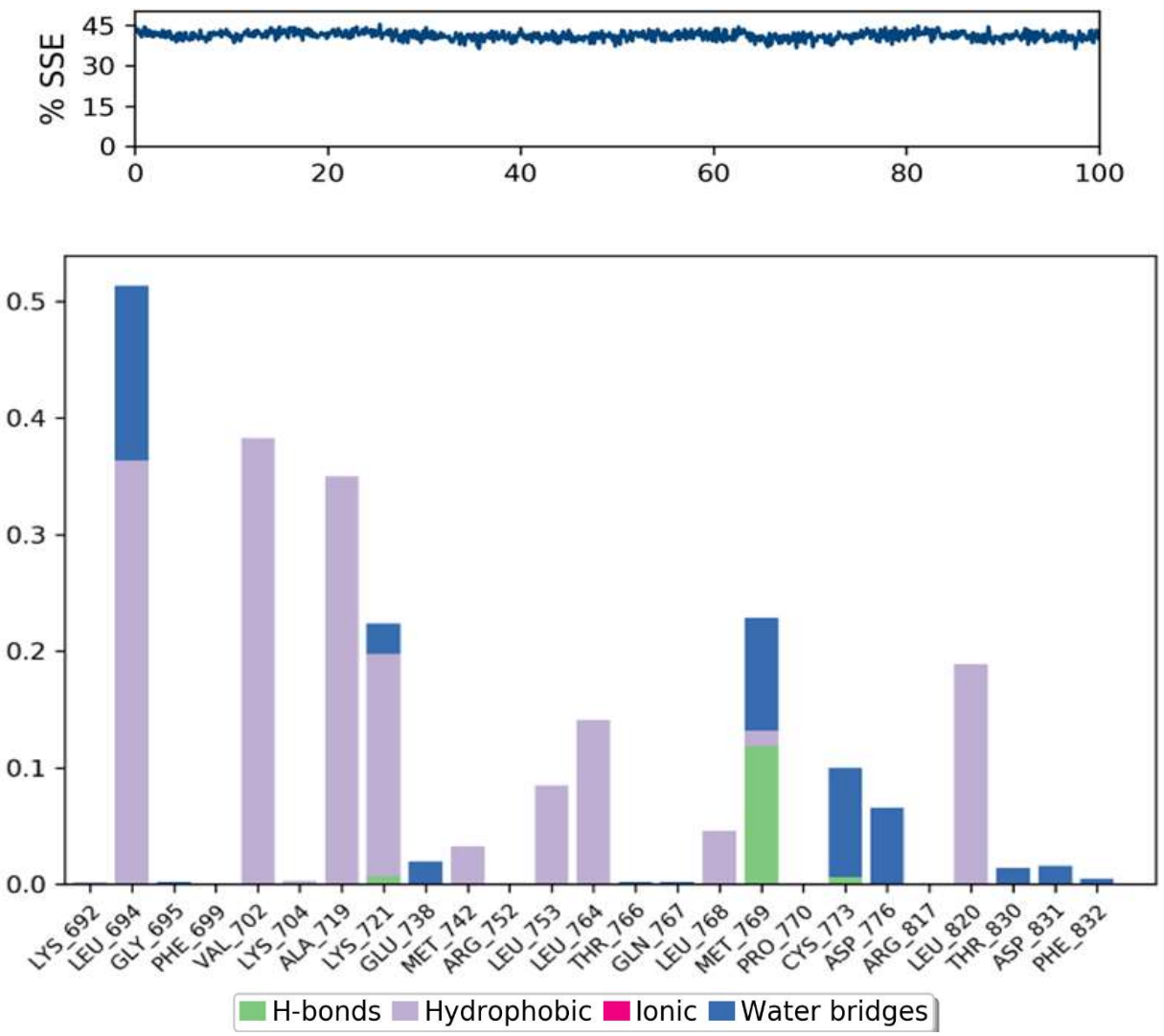

Figure 6: MD results of EGFR complexes. (A) Data of of the total contacts of both reference (up) and 23 (down) complexes with EGFR-TK. (B) Bar chart showing the normalized interactions during the trajectory with the specific interactions of both reference (up) and 23 analog (down) with the complex EGFR-TK.

3 Conclusion

In summary, we have designed and synthesized diarylpyrazole-based derivatives. A trial of complexation of pyranopyrazole analogs with gold metal through the terminal nitrile and amino groups resulted in ring opening and formation of benzylidene-2,4-dihydro-3*H*-pyrazol-3-one derivatives. This reaction was supported and confirmed with an X-ray analysis. All new derivatives were investigated for assay of their cytotoxicity against two different cancer cell lines of breast origin; (MCF-7 and MDA-MB-231). Also, the cytotoxicity against MCF-10A (as a human normal breast cell) was evaluated. The data of cytotoxic effect of all the novel derivatives showed active and selective analogs with IC_{50} values ranging from of 57.0-2.6 μM. In particular, pyrazolone derivative **23** was the most potent against invasive and non-invasive cancer types, with IC_{50} values of 2.60 and 5.14 μM, respectively. Moreover, rigid pyranopyrazole **20** was found to be selective against MCF-7 at 6.30 μM with very low normotoxicity. Moreover, EGFR-TK and CDK-9 enzymatic assays revealed sub-micromolar inhibitory activities of compound **23**. In addition, *in silico* docking was conducted, and their results confirmed consistent binding pattern of **23** with the target pockets of both biological targets. Finally, a molecular dynamic simulation experiment was introduced for the most active derivative **23** within EGFR-TK enzyme that showed a consistent target binding stability with range of proper types of interactions compatible with the docking results.

4 Experimental Section

4.1 Chemistry

All chemicals and reagents used in synthesis process are described in supplementary section in detail. In addition, the synthetic routs and spectroscopic characterization are presented in supplementary part.

4.2 General procedure for synthesis of 3-methyl-1,4-dihydropyrano[2,3-c]pyrazole derivatives and their spectral characterization (18-20) see supplementary section.

4.3 Reaction of compound 18 with gold (III) chloride hydrate

A reaction mixture of compound (**18**) (0.01 mol), gold (III) chloride hydrate (0.01 mol) and triethylamine (0.5 ml) was refluxed in an absolute ethyl alcohol solution (30 ml) for 1 hr. to give **21** in 66.2% afford final product as appeared in spectroscopic data.

4.4 Cytotoxicity evaluation

The cytotoxic effect was evaluated and determined by MTT colorimetric technique that was commonly known and previously reported [41,58–61]. Briefly, 1.2×10^4 to 1.5×10^4 of exponentially growing MCF-7 cells were seeded in 96-well plates containing RPMI-1640 medium (200 µl) and fetal bovine serum (10%). 96-well plates as six triplicates were prepared and the test compounds with different concentrations with range 0 to 50 μg/ml were then added into plates for all compound. Six vehicle controls with media or 0.5% DMSO were run for each 96-well plate as a control. Then, the number of viable cells were determined by the MTT test after incubation for 24 h.

In brief, the medium in the 96 well plates were replaced with fresh culture medium (100 L of RPMI 1640) without inclusion of phenol red, followed by addition of 10 µL of the MTT(12 mM) stock solution composed of (5 mg MTT/1 mL PBS) in each well, with the untreated controls. The well plates were incubated for 4 hrs under specific conditions (37 ^{o}C/5% CO_2). Removal of about 85-µl aliquot of the medium from each well was done and replaced by 50 µl of DMSO and thoroughly mixed with the pipette immediately prior to incubation at 37 ^{o}C for 10 minutes.

The optical density was then estimated by a microplate reader at 590 nm to determine the number of viable cells, and the percentage of viability was calculated using the formula:

: % viability = (O.D. Treated well/O.D. Control well) x 100 [62,63]. where OD denotes the mean optical density. The survival curve of each tumor cell line after treatment with

the specified compound was obtained by plotting the relationship between surviving cells and drug concentration. The 50% inhibitory concentration (IC_{50}), or the effective concentration required to produce toxicity in 50% of intact cells, was calculated using Graph Pad Prism software from graphic plots of the dose-response curve for each conc (San Diego, CA. USA).

4.5 EGFR-TK $^{wild\ type}$ assay

The methodology of assay occurred according to BPS Bioscience of the EGFR-TK kinase kit. In brief, 0.200 mg/mL EGFR-TK-ErbB1 (catalogue number PV3872) was employed. A solution of ATP as well as mixture of kinase/peptide were freshly and immediately prepared prior to the experiment, added to the plate wells and thoroughly mixed, followed by incubation at room temperature. for 1 hour. Following that, 5 ml of developing solution was added to each well. The plate was kept at room temperature for 1 hour before being read using an ELISA Reader (PerkinElmer, USA). Graph Pad Prism was used to fit the curves. Each experiment was carried out three times. Data from three independent experiments were represented as means ±SD.

4.6 Crystal structure analysis of a pyrazolone derivative, compound 21

Crystal data: $C_{17}H_{12}BrClN_2O$, M = 375.65. Monoclinic, space group Cc (no. 9), a = 10.5759(5), b = 14.0729(5), c = 10.3189(4) Å, β = 105.502(4)°, V = 1479.93(11) $Å^3$. Z = 4, Dc = 1.686 g cm^{-3}, F(000) = 752, T = 120(2) K, μ(Cu-Kα) = 54.7 cm^{-1}, λ(Cu-Kα) = 1.54184 Å.

The crystal was a red block. From a sample under Fomblin, one, *ca* 0.092 x 0.110 x 0.148 mm was supported on a tiny loop and fixed in the cold nitrogen stream on a Rigaku Oxford Diffraction SuperNova diffractometer, connected to Cu-Kα radiation, Atlas S2 detector and mirror monochromator. Results and statistics strength were calculated (University of Nottingham) by thin-slice ω-scans. Total number of reflections was

recorded to θ_{max} = 67.5°, it was 2634 of which 1690 were unique (Rint = 0.012); 1668 were 'observed' with $I > 2\sigma_I$.

Data processing was performed by applying the CrysAlisPro-CCD program [64]. The structure was assigned by the intrinsic phasing routines in the SHELXT program [65] and refined by full-matrix least-squares methods, on F^2's, in SHELXL [66]. The structure is disordered, with the major component overlaid with the minor component, and the Br and Cl atoms of the major molecule sharing the same sites as Cl(9) and Br(9) of the minor molecule. The non-hydrogen atoms were refined with anisotropic thermal parameters. The parent carbon atoms' Ueq values were made to be dependent on the Uiso values of the hydrogen atoms, which were included in idealized positions. . At the conclusion of the refinement, $wR_2 = 0.058$ and $R_1 = 0.023$ (2B) for all 1690 reflections weighted $w = [\sigma^2(F_o^2) + (0.0293P)^2 + 1.109P]^{-1}$ with $P = (F_o^2 + 2F_c^2)/3$; for the 'observed' data only, $R_1 = 0.022$. The Flack parameter, x, was 0.20(3) which suggests that the absolute configuration of the major component is correctly shown in the **Figure 3**. In the final difference map, the highest peak (*ca* 0.22 eÅ^{-3}) was near Br/Cl(9). Scattering factors for neutral atoms were brought from reference [67]. The software applied for current analysis have been mentioned before and were processed through WinGX [68] on a Dell Optiplex 780 PC at the University of East Anglia. The CIF file with these results has been deposited at the Cambridge Structure Database with CCDC deposition number 2152008.

4.7 Molecular docking

Molecular docking of the target compounds with the EGFR-TK protein enzyme (PDB ID: 1M17) was obtained in high resolution from the PDB server (http://www.pdb.org) using the most active compounds 21 and 22 derivatives. All docking calculations were performed using AutoDock 3.0 [69] and MOE software. The detailed protocol was followed as described in reference [7,70]. The inhibition constants were calculated using the binding energy file generated by docking experiments. MOE 2012.10 was employed

to generate the protein-ligand interaction plots. The default parameter settings were used.

A grid box size of 90×90×90 points with a spacing of 0.375 Å between the grid points was generated that covered almost the entire protein surface. Lamarckian GA was employed for the conformational space search with initial population set to 150, and fitness function evaluations set to 25000000. The most abundant low-energy clusters were selected for analysis.High-scoring binding poses were selected based on visual inspection.

4.8 Molecular dynamics simulation

Molecular dynamics simulations were performed by applying using templates of the 3D structure crystal of EGFR-TK complexed with the target active compound 23 (PDB ID: 1M17) compared to co-crystallized ligand. The simulation was run with the Desmond 3.8 package [71,72] and the OPLS2005 forcefield. The computational hardware in this simulation was SGI Rackalbe RP2 Standard-Depth Servers C2108-RP2 (Intel Xeon Processor E5-2670, 16CPU/node) at AIST. The initial docked model structure was refined in Maestro (Schrödinger, LLC) using the protein preparation wizard and placed into TIP3P water molecules solvated with 0.15 M NaCl. Following model minimization and relaxation, the production molecular dynamics phase was carried out in an isothermal-isobaric (NpT) ensemble at 300 K and 1 bar for three independent 100 ns simulations.

Acknowledgment: This work was funded by the Deanship of Scientific Research at Jouf University under Grant Number (DSR2022-RG-0151). MAS is thankful to AvH.

Conflicts of Interest: The authors declare no conflict of interest

References

[1] The World Health Organization, Cancer, (2022). https://www.who.int/news-room/fact-sheets/detail/cancer (accessed May 12, 2022).

[2] R. Ali, M.K. Wendt, The paradoxical functions of EGFR during breast cancer progression, Signal Transduct. Target. Ther. 2 (2017) 16042. https://doi.org/10.1038/sigtrans.2016.42.

[3] E. Mishani, G. Abourbeh, M. Eiblmaier, C. Anderson, Imaging of EGFR and EGFR Tyrosine Kinase Overexpression in Tumors by Nuclear Medicine Modalities, Curr. Pharm. Des. 14 (2008) 2983–2998. https://doi.org/10.2174/138161208786404326.

[4] M.A.S. Abourehab, A.M. Alqahtani, B.G.M. Youssif, A.M. Gouda, Globally Approved EGFR Inhibitors: Insights into Their Syntheses, Target Kinases, Biological Activities, Receptor Interactions, and Metabolism, Molecules. 26 (2021) 6677. https://doi.org/10.3390/molecules26216677.

[5] A. Canonici, A.L. Browne, M.F.K. Ibrahim, K.P. Fanning, S. Roche, N.T. Conlon, F. O'Neill, J. Meiller, M. Cremona, C. Morgan, B.T. Hennessy, A.J. Eustace, F. Solca, N. O'Donovan, J. Crown, Combined targeting EGFR and SRC as a potential novel therapeutic approach for the treatment of triple negative breast cancer, Ther. Adv. Med. Oncol. 12 (2020) 175883591989754. https://doi.org/10.1177/1758835919897546.

[6] T. Yamaoka, S. Kusumoto, K. Ando, M. Ohba, T. Ohmori, Receptor Tyrosine Kinase-Targeted Cancer Therapy, Int. J. Mol. Sci. 19 (2018) 3491. https://doi.org/10.3390/ijms19113491.

[7] A.A. Gaber, A.M. El‐Morsy, F.F. Sherbiny, A.H. Bayoumi, K.M. El‐Gamal, K. El‐Adl, A.A. Al‐Karmalawy, R.R. Ezz Eldin, M.A. Saleh, H.S. Abulkhair, Pharmacophore‐linked pyrazolo[3,4‐d]pyrimidines as EGFR‐TK inhibitors: Synthesis, anticancer evaluation, pharmacokinetics, and in silico mechanistic studies, Arch. Pharm. (Weinheim). (2021). https://doi.org/10.1002/ardp.202100258.

[8] J. Kang, Z. Guo, H. Zhang, R. Guo, X. Zhu, X. Guo, Dual Inhibition of EGFR and IGF-1R Signaling Leads to Enhanced Antitumor Efficacy against Esophageal Squamous Cancer, Int. J. Mol. Sci. 23 (2022) 10382. https://doi.org/10.3390/ijms231810382.

[9] S.-S. Cheng, Y.-Q. Qu, J. Wu, G.-J. Yang, H. Liu, W. Wang, Q. Huang, F. Chen, G. Li, C.-Y. Wong, V.K.W. Wong, D.-L. Ma, C.-H. Leung, Inhibition of the CDK9–cyclin T1 protein–protein interaction as a new approach against triple-negative breast cancer, Acta Pharm. Sin. B. 12 (2022) 1390–1405. https://doi.org/10.1016/j.apsb.2021.10.024.

[10] P. Gupta, S. Narayanan, D.-H. Yang, CDK Inhibitors as Sensitizing Agents for Cancer Chemotherapy, in: Protein Kinase Inhib. as Sensitizing Agents Chemother., Elsevier, 2019: pp. 125–

149. https://doi.org/10.1016/B978-0-12-816435-8.00009-2.

[11] D. Brisard, F. Eckerdt, L.A. Marsh, G.T. Blyth, S. Jain, M. Cristofanilli, D. Horiuchi, L.C. Platanias, Antineoplastic effects of selective CDK9 inhibition with atuveciclib on cancer stem-like cells in triple-negative breast cancer, Oncotarget. 9 (2018) 37305–37318. https://doi.org/10.18632/oncotarget.26468.

[12] M. Zhang, L. Zhang, R. Hei, X. Li, H. Cai, X. Wu, Q. Zheng, C. Cai, CDK inhibitors in cancer therapy, an overview of recent development., Am. J. Cancer Res. 11 (2021) 1913–1935. http://www.ncbi.nlm.nih.gov/pubmed/34094661.

[13] P. Mitra, R.-M. Yang, J. Sutton, R.G. Ramsay, T.J. Gonda, CDK9 inhibitors selectively target estrogen receptor-positive breast cancer cells through combined inhibition of MYB and MCL-1 expression, Oncotarget. 7 (2016) 9069–9083. https://doi.org/10.18632/oncotarget.6997.

[14] A. Bolomsky, M. Vogler, M.C. Köse, C.A. Heckman, G. Ehx, H. Ludwig, J. Caers, MCL-1 inhibitors, fast-lane development of a new class of anti-cancer agents, J. Hematol. Oncol. 13 (2020) 173. https://doi.org/10.1186/s13045-020-01007-9.

[15] M. Mantzanidou, E. Pontiki, D. Hadjipavlou-Litina, Pyrazoles and Pyrazolines as Anti-Inflammatory Agents, Molecules. 26 (2021) 3439. https://doi.org/10.3390/molecules26113439.

[16] H. Abul-Khair, S. Elmeligie, A. Bayoumi, A. Ghiaty, A. El-Morsy, M.H. Hassan, Synthesis and evaluation of some new (1,2,4) triazolo(4,3-a)quinoxalin- 4(5h)-one derivatives as AMPA receptor antagonists, J. Heterocycl. Chem. 50 (2013) 1202–1208. https://doi.org/10.1002/jhet.714.

[17] H.S. Abulkhair, S. Elmeligie, A. Ghiaty, A. El-Morsy, A.H. Bayoumi, H.E.A. Ahmed, K. El-Adl, M.F. Zayed, M.H. Hassan, E.N. Akl, M.S. El-Zoghbi, In vivo- and in silico-driven identification of novel synthetic quinoxalines as anticonvulsants and AMPA inhibitors, Arch. Pharm. (Weinheim). 354 (2021) 2000449. https://doi.org/10.1002/ardp.202000449.

[18] D.M. Khaled, M.E. Elshakre, M.A. Noamaan, H. Butt, M.M. Abdel Fattah, D.A. Gaber, A Computational QSAR, Molecular Docking and In Vitro Cytotoxicity Study of Novel Thiouracil-Based Drugs with Anticancer Activity against Human-DNA Topoisomerase II, Int. J. Mol. Sci. 23 (2022) 11799. https://doi.org/10.3390/ijms231911799.

[19] P. saradhi chandavaram, S.J. Maddirala, S. Vidavalur, N. Somaiah, Design, synthesis and biological evaluation of isoxazole bearing N-Arylpyrazole derivatives as anticancer agents, Chem. Data Collect. 41 (2022) 100938. https://doi.org/10.1016/j.cdc.2022.100938.

[20] M.J.V. da Silva, A.P. Jacomini, M.C. Figueiredo, D.F. Back, M.A. Foglio, A.L.T.G. Ruiz, F.R. Paula, F.A. Rosa, Efficient synthesis and antitumor evaluation of 4-aminomethyl-N-arylpyrazoles:

Discovery of potent and selective agents for ovarian cancer, Bioorg. Med. Chem. 29 (2021) 115835. https://doi.org/10.1016/j.bmc.2020.115835.

[21] A. Aljuhani, H.E.A. Ahmed, S.K. Ihmaid, A.M. Omar, S.S. Althagfan, Y.M. Alahmadi, I. Ahmad, H. Patel, S. Ahmed, M.A. Almikhlafi, A.M. El-Agrody, M.F. Zayed, S.A. Turkistani, S.H. Abulkhair, M. Almaghrabi, S.A. Salama, A.A. Al-Karmalawy, H.S. Abulkhair, In vitro and computational investigations of novel synthetic carboxamide-linked pyridopyrrolopyrimidines with potent activity as SARS-CoV-2-M Pro inhibitors, RSC Adv. 12 (2022) 26895–26907. https://doi.org/10.1039/D2RA04015H.

[22] R. Singh, R. Bansal, 16,17-N′-(alky/arylsulfonyl)pyrazoline substituted neuroprotective heterosteroids: Synthesis, molecular docking and preclinical efficacy/toxicity studies in rodents, Steroids. 148 (2019) 114–124. https://doi.org/10.1016/j.steroids.2019.05.002.

[23] E.Z. Mohammed, W.R. Mahmoud, R.F. George, G.S. Hassan, F.A. Omar, H.H. Georgey, Synthesis, in vitro anticancer activity and in silico studies of certain pyrazole-based derivatives as potential inhibitors of cyclin dependent kinases (CDKs), Bioorg. Chem. 116 (2021) 105347. https://doi.org/10.1016/j.bioorg.2021.105347.

[24] M.M.F. Ismail, D.H. Soliman, R. Sabour, A.M. Farrag, Synthesis of new arylazopyrazoles as apoptosis inducers: Candidates to inhibit proliferation of MCF‐7 cells, Arch. Pharm. (Weinheim). 354 (2021) 2000214. https://doi.org/10.1002/ardp.202000214.

[25] M.M.F. Ismail, D.H. Soliman, R. Sabour, A.M. Farrag, Synthesis of new arylazopyrazoles as apoptosis inducers: Candidates to inhibit proliferation of MCF‐7 cells, Arch. Pharm. (Weinheim). 354 (2021) 2000214. https://doi.org/10.1002/ardp.202000214.

[26] A.M. Fouda, M.A.A. El-Nassag, A.A. Elhenawy, A.A. Shati, M.Y. Alfaifi, S.E.I. Elbehairi, M.M. Alam, A.M. El-Agrody, Synthesis of 1,4-dihydropyrano[2,3-c]pyrazole derivatives and exploring molecular and cytotoxic properties based on DFT and molecular docking studies, J. Mol. Struct. 1249 (2022) 131555. https://doi.org/10.1016/j.molstruc.2021.131555.

[27] A.M. El-Agrody, A.M. Fouda, H.M. Mohamed, M.Y. Alshahrani, H.A. Ghabbour, A.E.-G.E. Amr, R.M. Okasha, A.M. Naglah, A.A. Almehizia, A.A. Elhenawy, The Crystal Structure of 2-Amino-4-(2,3-Dichlorophenyl)-6-Methoxy-4H-Benzo[h]chromene-3-Carbonitrile: Antitumor and Tyrosine Kinase Receptor Inhibition Mechanism Studies, Crystals. 12 (2022) 737. https://doi.org/10.3390/cryst12050737.

[28] R.M. Okasha, A.M. Fouda, M.A. Bajaber, H.A. Ghabbour, A.E.-G. E. Amr, A.M. Naglah, A.A. Almehizia, A.A. Elhenawy, A.M. El-Agrody, The Crystal Structure of 3-Amino-1-(4-Chlorophenyl)-

9-Methoxy-1H-Benzo[f]Chromene-2-Carbonitrile: Antimicrobial Activity and Docking Studies, Crystals. 12 (2022) 982. https://doi.org/10.3390/cryst12070982.

[29] H.K.A. El-Mawgoud, H.A.M. Radwan, A.M. Fouda, F. El-Mariah, A.A. Elhenawy, A.E. Amr, A.A. Almehizia, H.A. Ghabbour, A.M. El-Agrody, Synthesis, cytotoxic activity, crystal structure, DFT, molecular docking study of some heterocyclic compounds incorporating benzo[f]chromene moieties, J. Mol. Struct. 1260 (2022) 132829. https://doi.org/10.1016/j.molstruc.2022.132829.

[30] L. Massai, D. Cirri, E. Michelucci, G. Bartoli, A. Guerri, M.A. Cinellu, F. Cocco, C. Gabbiani, L. Messori, Organogold(III) compounds as experimental anticancer agents: chemical and biological profiles, BioMetals. 29 (2016) 863–872. https://doi.org/10.1007/s10534-016-9957-x.

[31] N. Mirzadeh, T.S. Reddy, S.K. Bhargava, Advances in diphosphine ligand-containing gold complexes as anticancer agents, Coord. Chem. Rev. 388 (2019) 343–359. https://doi.org/10.1016/j.ccr.2019.02.027.

[32] H. Schmidbaur, A. Schier, Gold η 2 -Coordination to Unsaturated and Aromatic Hydrocarbons: The Key Step in Gold-Catalyzed Organic Transformations, Organometallics. 29 (2010) 2–23. https://doi.org/10.1021/om900900u.

[33] A.S.K. Hashmi, M. Rudolph, Gold catalysis in total synthesis, Chem. Soc. Rev. 37 (2008) 1766. https://doi.org/10.1039/b615629k.

[34] R. Visbal, S. Graus, R.P. Herrera, M.C. Gimeno, Gold Catalyzed Multicomponent Reactions beyond A3 Coupling, Molecules. 23 (2018) 2255. https://doi.org/10.3390/molecules23092255.

[35] X.-Z. Shu, X.-Y. Liu, H.-Q. Xiao, K.-G. Ji, L.-N. Guo, C.-Z. Qi, Y.-M. Liang, Gold-Catalyzed Tandem Cycloisomerization of Alkynyloxiranes with Nucleophiles: An Efficient Approach to 2,5-Disubstituted Furans, Adv. Synth. Catal. 349 (2007) 2493–2498. https://doi.org/10.1002/adsc.200700319.

[36] Y. Tominaga, M. Kawabe, A. Hosomi, Synthesis of 4-methylthio-2(1 H)-pyridone derivatives using ketene dithioacetals, J. Heterocycl. Chem. 24 (1987) 1325–1331. https://doi.org/10.1002/jhet.5570240519.

[37] Z. Rappoport, D. Ladkani, Nucleophilic attacks on carbon–carbon double bonds. Part XX. Reaction of active methylene compounds with electrophilic olefins. Formation of substituted 2-amino-4-cyano-4H-pyrans, J. Chem. Soc., Perkin Trans. 1. (1974) 2595–2601. https://doi.org/10.1039/P19740002595.

[38] V.D. Dyachenko, A.D. Dyachenko, A.N. Chernega, Synthesis of Substituted 1,3-Cyclohexadienes, Pyridine-2(1H)-thiones, and Thieno[2,3-d]pyrimidine- 4(3H)-thiones by the Michael Reaction, Russ.

J. Org. Chem. 40 (2004) 397–406. https://doi.org/10.1023/B:RUJO.0000034978.81993.bd.

[39] M. Elgaafary, A.M. Fouda, H.M. Mohamed, A. Hamed, H.K.A. El-Mawgoud, L. Jin, J. Ulrich, T. Simmet, T. Syrovets, A.M. El-Agrody, Synthesis of β-Enaminonitrile-Linked 8-Methoxy-1H-Benzo[f]Chromene Moieties and Analysis of Their Antitumor Mechanisms, Front. Chem. 9 (2021). https://doi.org/10.3389/fchem.2021.759148.

[40] M. El Gaafary, J. Lehner, A.M. Fouda, A. Hamed, J. Ulrich, T. Simmet, T. Syrovets, A.M. El-Agrody, Synthesis and evaluation of antitumor activity of 9-methoxy-1H-benzo[f]chromene derivatives, Bioorg. Chem. 116 (2021) 105402. https://doi.org/10.1016/j.bioorg.2021.105402.

[41] T. Mosmann, Rapid colorimetric assay for cellular growth and survival: Application to proliferation and cytotoxicity assays, J. Immunol. Methods. 65 (1983) 55–63. https://doi.org/10.1016/0022-1759(83)90303-4.

[42] H.G. Ezzat, A.H. Bayoumi, F.F. Sherbiny, A.M. El-Morsy, A. Ghiaty, M. Alswah, H.S. Abulkhair, Design, synthesis, and molecular docking studies of new [1,2,4]triazolo[4,3-a]quinoxaline derivatives as potential A2B receptor antagonists, Mol. Divers. 25 (2021) 291–306. https://doi.org/10.1007/s11030-020-10070-w.

[43] A. Turky, A.H. Bayoumi, A. Ghiaty, A.S. El-Azab, A. A.-M. Abdel-Aziz, H.S. Abulkhair, Design, synthesis, and antitumor activity of novel compounds based on 1,2,4-triazolophthalazine scaffold: Apoptosis-inductive and PCAF-inhibitory effects, Bioorg. Chem. 101 (2020) 104019. https://doi.org/10.1016/j.bioorg.2020.104019.

[44] L. Xue, S. Chiu, N.L. Oleinick, Staurosporine-induced death of MCF-7 human breast cancer cells: a distinction between caspase-3-dependent steps of apoptosis and the critical lethal lesions, Exp. Cell Res. 283 (2003) 135–145. https://doi.org/10.1016/S0014-4827(02)00032-0.

[45] E.M. Othman, E.A. Fayed, E.M. Husseiny, H.S. Abulkhair, Apoptosis induction, PARP-1 inhibition, and cell cycle analysis of leukemia cancer cells treated with novel synthetic 1,2,3-triazole-chalcone conjugates, Bioorg. Chem. 123 (2022) 105762. https://doi.org/10.1016/j.bioorg.2022.105762.

[46] P.D. Leeson, B. Springthorpe, The influence of drug-like concepts on decision-making in medicinal chemistry, Nat. Rev. Drug Discov. 6 (2007) 881–890. https://doi.org/10.1038/nrd2445.

[47] M.H. El-Shershaby, A. Ghiaty, A.H. Bayoumi, H.E.A. Ahmed, M.S. El-Zoghbi, K. El-Adl, H.S. Abulkhair, 1,2,4-Triazolo[4,3- c]quinazolines: a bioisosterism-guided approach towards the development of novel PCAF inhibitors with potential anticancer activity, New J. Chem. 45 (2021) 11136–11152. https://doi.org/10.1039/D1NJ00710F.

[48] K. El-Adl, H. Sakr, S.S.A. El-Hddad, A.G.A. El-Helby, M. Nasser, H.S. Abulkhair, Design, synthesis,

docking, ADMET profile, and anticancer evaluations of novel thiazolidine-2,4-dione derivatives as VEGFR-2 inhibitors, Arch. Pharm. (Weinheim). 354 (2021) 2000491. https://doi.org/10.1002/ardp.202000491.

[49] O. Kutkat, Y. Moatasim, A.A. Al‐Karmalawy, H.S. Abulkhair, M.R. Gomaa, A.N. El-Taweel, N.M. Abo Shama, M. GabAllah, D.B. Mahmoud, G. Kayali, M.A. Ali, A. Kandeil, A. Mostafa, Robust antiviral activity of commonly prescribed antidepressants against emerging coronaviruses: in vitro and in silico drug repurposing studies, Sci. Rep. 12 (2022) 12920. https://doi.org/10.1038/s41598-022-17082-6.

[50] M.I.A. Hamed, K.M. Darwish, R. Soltane, A. Chrouda, A. Mostafa, N.M. Abo Shama, S.S. Elhady, H.S. Abulkhair, A.E. Khodir, A.A. Elmaaty, A.A. Al-karmalawy, β-Blockers bearing hydroxyethylamine and hydroxyethylene as potential SARS-CoV-2 Mpro inhibitors: rational based design, in silico , in vitro , and SAR studies for lead optimization, RSC Adv. 11 (2021) 35536–35558. https://doi.org/10.1039/D1RA04820A.

[51] K. El-Adl, A.G.A. El-Helby, H. Sakr, R.R. Ayyad, H.A. Mahdy, M. Nasser, H.S. Abulkhair, S.S.A. El-Hddad, Design, synthesis, molecular docking, anticancer evaluations, and in silico pharmacokinetic studies of novel 5-[(4-chloro/2,4-dichloro)benzylidene]thiazolidine-2,4-dione derivatives as VEGFR-2 inhibitors, Arch. Pharm. (Weinheim). 354 (2021) 2000279. https://doi.org/10.1002/ardp.202000279.

[52] S. Ihmaid, H. Ahmed, M. Zayed, The Design and Development of Potent Small Molecules as Anticancer Agents Targeting EGFR TK and Tubulin Polymerization, Int. J. Mol. Sci. 19 (2018) 408. https://doi.org/10.3390/ijms19020408.

[53] M. Alswah, A. Bayoumi, K. Elgamal, A. Elmorsy, S. Ihmaid, H. Ahmed, Design, Synthesis and Cytotoxic Evaluation of Novel Chalcone Derivatives Bearing Triazolo[4,3-a]-quinoxaline Moieties as Potent Anticancer Agents with Dual EGFR Kinase and Tubulin Polymerization Inhibitory Effects, Molecules. 23 (2017) 48. https://doi.org/10.3390/molecules23010048.

[54] H.E.A. Ahmed, S.K. Ihmaid, A.M. Omar, A.M. Shehata, H.S. Rateb, M.F. Zayed, S. Ahmed, M.M. Elaasser, Design, synthesis, molecular docking of new lipophilic acetamide derivatives affording potential anticancer and antimicrobial agents, Bioorg. Chem. 76 (2018) 332–342. https://doi.org/10.1016/j.bioorg.2017.11.019.

[55] J. Stamos, M.X. Sliwkowski, C. Eigenbrot, Structure of the Epidermal Growth Factor Receptor Kinase Domain Alone and in Complex with a 4-Anilinoquinazoline Inhibitor, J. Biol. Chem. 277 (2002) 46265–46272. https://doi.org/10.1074/jbc.M207135200.

[56] H. Mazal, H. Aviram, I. Riven, G. Haran, Effect of ligand binding on a protein with a complex folding landscape, Phys. Chem. Chem. Phys. 20 (2018) 3054–3062. https://doi.org/10.1039/C7CP03327C.

[57] S. Yousuf, K.M. Khan, U. Salar, S. Chigurupati, M.T. Muhammad, A. Wadood, M. Aldubayan, V. Vijayan, M. Riaz, S. Perveen, 2'-Aryl and 4'-arylidene substituted pyrazolones: As potential α-amylase inhibitors, Eur. J. Med. Chem. 159 (2018) 47–58. https://doi.org/10.1016/j.ejmech.2018.09.052.

[58] E.M. Othman, E.A. Fayed, E.M. Husseiny, H.S. Abulkhair, Rationale design, synthesis, cytotoxicity evaluation, and in silico mechanistic studies of novel 1,2,3-triazoles with potential anticancer activity, New J. Chem. 46 (2022) 12206–12216. https://doi.org/10.1039/d2nj02061k.

[59] E.M. Othman, E.A. Fayed, E.M. Husseiny, H.S. Abulkhair, The effect of novel synthetic semicarbazone- and thiosemicarbazone-linked 1,2,3-triazoles on the apoptotic markers, VEGFR-2, and cell cycle of myeloid leukemia, Bioorg. Chem. 127 (2022) 105968. https://doi.org/10.1016/j.bioorg.2022.105968.

[60] F. Khedr, M.K. Ibrahim, I.H. Eissa, H.S. Abulkhair, K. El-Adl, Phthalazine-based VEGFR-2 inhibitors: Rationale, design, synthesis, in silico, ADMET profile, docking, and anticancer evaluations, Arch. Pharm. (Weinheim). 354 (2021) e2100201. https://doi.org/10.1002/ardp.202100201.

[61] I. Husain, A. Sharma, S. Kumar, F. Malik, Purification and characterization of glutaminase free asparaginase from Pseudomonas otitidis: Induce apoptosis in human leukemia MOLT-4 cells, Biochimie. 121 (2016) 38–51. https://doi.org/10.1016/j.biochi.2015.11.012.

[62] K. Bala, I. Husain, A. Sharma, Arginine deaminase from Pseudomonas aeruginosa PS2: purification, biochemical characterization and in-vitro evaluation of anticancer activity, 3 Biotech. 10 (2020) 226. https://doi.org/10.1007/s13205-020-02212-6.

[63] A. Sharma, I. Husain, Evaluation of Antitumor Activity of Glutaminase-Free Periplasmic Asparaginase from Indigenous Bacterial Isolates as Candidates for Cancer Therapy, Proc. Natl. Acad. Sci. India Sect. B Biol. Sci. 87 (2017) 997–1004. https://doi.org/10.1007/s40011-015-0681-z.

[64] CrysAlis, Data Collection and Processing Software for Agilent X-ray Diffractometers, (2013). https://www.agilent.com/cs/library/usermanuals/Public/CrysAlis_Pro_User_Manual.pdf.

[65] G.M. Sheldrick, SHELXT – Integrated space-group and crystal-structure determination, Acta Crystallogr. Sect. A Found. Adv. 71 (2015) 3–8. https://doi.org/10.1107/S2053273314026370.

[66] M. Beller, T.H. Riermeier, W. Mägerlein, T.E. Müller, W. Scherer, Chemistry of chelate-stabilized aryloxopalladium(II) complexes: syntheses, X-ray crystal structures and formation of C · H···O

hydrogen-bonds, Polyhedron. 17 (1998) 1165–1176. https://doi.org/10.1016/S0277-5387(97)00504-4.

[67] E. Prince, International Tables for Crystallography, Volume C, 3rd Edition, Mathematical, Physical and Chemical Tables, 1st ed., Wiley Online Library, 2004. https://www.wiley.com/en-us/International+Tables+for+Crystallography%2C+Volume+C%2C+3rd+Edition%2C+Mathematical%2C+Physical+and+Chemical+Tables-p-9780470710296.

[68] L.J. Farrugia, WinGX and ORTEP for Windows : an update, J. Appl. Crystallogr. 45 (2012) 849–854. https://doi.org/10.1107/S0021889812029111.

[69] A.A. Zaki, M.M.Y. Kaddah, H.S. Abulkhair, A. Ashour, Unravelling the antifungal and antiprotozoal activities and LC-MS/MS quantification of steroidal saponins isolated from Panicum turgidum, RSC Adv. 12 (2022) 2980–2991. https://doi.org/10.1039/D1RA08532H.

[70] H.S. Abulkhair, A. Turky, A. Ghiaty, H.E.A. Ahmed, A.H. Bayoumi, Novel triazolophthalazine-hydrazone hybrids as potential PCAF inhibitors: Design, synthesis, in vitro anticancer evaluation, apoptosis, and molecular docking studies, Bioorg. Chem. 100 (2020) 103899. https://doi.org/10.1016/j.bioorg.2020.103899.

[71] K.J. Bowers, D.E. Chow, H. Xu, R.O. Dror, M.P. Eastwood, B.A. Gregersen, J.L. Klepeis, I. Kolossvary, M.A. Moraes, F.D. Sacerdoti, J.K. Salmon, Y. Shan, D.E. Shaw, Scalable Algorithms for Molecular Dynamics Simulations on Commodity Clusters, in: ACM/IEEE SC 2006 Conf., IEEE, 2006: pp. 43–43. https://doi.org/10.1109/SC.2006.54.

[72] M.M. Hammoud, M. Khattab, M. Abdel-Motaal, J. Van der Eycken, R. Alnajjar, H. Abulkhair, A.A. Al - Karmalawy, Synthesis, structural characterization, DFT calculations, molecular docking, and molecular dynamics simulations of a novel ferrocene derivative to unravel its potential antitumor activity, J. Biomol. Struct. Dyn. (2022). https://doi.org/10.1080/07391102.2022.2082533.